Reactive plasma sputtering deposition of polycrystalline GaN thin films on silicon substrates at room temperature

Lakshman Srinivasan, Cyril Jadaud, François Silva, Jean-Charles Vanel, Jean-Luc Maurice, Erik Johnson, Pere Roca i Cabarrocas, Karim Ouaras

Reactive Plasma Sputtering Deposition of Polycrystalline GaN Thin Films on Silicon Substrates at Room Temperature

Lakshman Srinivasan[1,2], Cyril Jadaud[1], François Silva[1], Jean-Charles Vanel[1], Jean-Luc Maurice[1], Erik Johnson[1], Pere Roca i Cabarrocas[1,2], Karim Ouaras[1,*]

[1]*LPICM, CNRS, Ecole polytechnique, Institut polytechnique de Paris 91120 Palaiseau. France.*

[2] *IPVF, Institut Photovoltaïque d'Ile-de-France, 18 Bd Thomas Gobert, 91120 Palaiseau, France.*

karim.ouaras@polytechnique.edu

Keywords – Gallium Nitride (GaN), Plasma, Magnetron Sputtering, Optical Emission Spectroscopy, Wurtzite GaN

Abstract

We report on the successful growth of polycrystalline GaN thin films on Si (100) substrates at room temperature (without intentional heating) using radiofrequency reactive magnetron sputtering. We use Ar and N_2 as the main sputtering and N-atom precursor gas sources, respectively, and a gallium cathode as the Ga-atom source. We focus here on studying the effect of the working pressure as it is found to be the parameter that plays the most influential role on the crystalline quality of the thin films in the investigated range (20 to 95 mTorr). The morphology, microstructure, and composition profile of the GaN thin films are analyzed using a set of *ex-situ* solid-state characterization techniques. This study reveals that for process pressures below 50 mTorr, the resulting films possess an amorphous nature, while for process pressures above that they become polycrystalline. Most of the crystalline films are found to be nanostructured with grain sizes typically ranging from 10 to 30 nm in size. The highest growth rate of ~ 2.9 Å/s is obtained for the deposition carried out at 50 mTorr. At this pressure, the films exhibit the best crystallinity with a dominant wurtzite hexagonal structure. The elemental distribution of Ga and N throughout the growth profile is uniform with a sharp interface at the substrate demonstrating one of the interests in working at low temperature to avoid melt-back etching, a destructive reaction between gallium and silicon, that usually takes place at high temperature.

I. Introduction

Semiconductors such as GaN, AlN and InN belonging to the III-nitrides group have been extensively studied in the past few decades due to their complementary and/or superior optoelectronic properties with respect to silicon. These materials, in high-quality epitaxial forms, have rapidly matured in numerous applications encompassing light-emitting diodes (LEDs)[1], laser diodes (LDs)[2], field effect transistors (FETs)[3], etc. Among the aforementioned wide band gap semiconductors, GaN has attracted the most attention owing to its direct band gap of 3.4 eV, high electron mobility, good thermal stability, and elevated mechanical hardness. It is considered as a key material in high-power and high-frequency electronic applications[4].

GaN based devices are usually grown by CVD on substrates such as sapphire and SiC due to the lack of ingot-based GaN substrates, which cannot be produced through melting in contrast to silicon. Even though sapphire and SiC, which have a moderate lattice mismatch with GaN, appear to be the most convenient substrates, they remain expensive. One of the best options would be to use silicon substrates, as they are cheap and abundant. However, the quality of GaN films grown on Si remains poor when compared to those grown on sapphire, due to the large lattice mismatch (~ 17 %) that causes a high dislocation density in the grown films[5]. Therefore, finding strategies towards the integration of high power electronics (GaN) with current Si-based electronics has become a very active topic of research[6].

Among the conventional epitaxial processes used to grow GaN, metal organic chemical vapor deposition (MOCVD) and molecular beam epitaxy (MBE) are the most used and studied in both academic and industrial

research labs. These methods do produce high quality GaN layers, yet they have their own drawbacks. For example, MOCVD uses toxic gases as precursors and operates at very high temperatures (~1000 °C) to enable the pyrolysis of precursors[7]. Furthermore, MBE faces issues of (i) high cost because of the utilization of ultra-high vacuum pumping, and (ii) scalability[8]. One of the main drawbacks associated with these processing methods is that they operate at high temperature. This induces thermal mismatch strain due to large thermal expansion coefficient difference between GaN ($\alpha_{298.2}$ = 5.59x10^{-6} K^{-1}) and Si ($\alpha_{298.2}$ = 2.59 x 10^{-6} K^{-1}) that causes film cracking and wafer bowing upon cooling[6]. Moreover, the direct growth of GaN on Si at temperatures above 500 °C leads to meltback etching, a deteriorating chemical reaction that occurs between Ga and Si, and which limits the development of GaN on Si substrates[9]. A potential solution to avoid those problems is to resort to a lower temperature processing method such as sputtering. Low-temperature sputtering[10–14], even though it might not be able to produce high-quality crystalline films as conventional epitaxial processes , it possesses several advantages over these methods: (i) it is a highly reactive medium in which not only radicals but also charged species participate in the growth while keeping a global (gas) temperature that may be as low as room temperature; (ii) it provides the ability to tune the flux or energy of the active species reaching the substrate, enabling a better control of both the adhesion and quality of the films; (iii) it does not require the use of toxic or organic gases; (iv) it does not require ultra-high vacuum and (v) it is widely used in industry so it has the potential for scaling up. In the literature, some works have been done on optimizing the sputtering process and the subsequent deposition of epitaxial GaN layers[12,15]. However, in these works, the substrate temperature usually exceeded 700°C. The main limitations of the deposition at temperatures lower than 700 °C is the difficulty to crystallize the material and hence an amorphous layer or a crystalline layer of poor quality is usually obtained. Therefore, additional annealing steps are usually required, compromising the benefit of using plasmas as a way to both reduce the thermal budget and to mitigate the thermal mismatch issue. There is still an effort to be made on the control of the plasma process in order to fully exploit its potential to reduce the process temperature as much as possible, while keeping the crystalline quality of the thin films as high as possible.

Over the past few decades, the interest in polycrystalline GaN is slowly growing since its deposition conditions are more lenient than those of epitaxial GaN. The ability to use diverse substrates, to deposit at lower temperatures and to be able to grow GaN directly on the substrate without using a buffer layer, are some of the important reasons for this interest. A limited amount of research has been done so far to study the growth of polycrystalline GaN using plasmas at substrate temperatures ranging from room temperature up to 550°C[16–19]. Recent works by H. Wei et al (2019)[20] and P. Qui et al (2020)[21] demonstrate the use of polycrystalline GaN as an electron transport layer (ETL) in perovskite solar cells, paving its way towards photovoltaic applications. Reducing the growth temperature could also open the door to numerous applications requiring flexible devices that use thermally sensitive substrates[22].

In this work, we demonstrate that the growth of polycrystalline GaN thin films on silicon substrate can be achieved, at room temperature, when plasma sputtering is used. In section 2, we describe the plasma set-up and characterizations. In section 3, we present the results and discussion regarding the global analysis of the plasma and the properties of the GaN thin films.

II. Experimental

A. Plasma sputtering set-up.

The growth experiments were performed in a custom-built sputtering system (**Figure 1**). The PVD (Physical Vapor Deposition) reactor consists of a six-way cross stainless-steel chamber that possesses several optical ports to perform spectroscopic analysis. It uses a 2"-circular commercial magnetron sputtering source (Torus® - Kurt J. Lesker Company) that was customized to integrate a specific crucible to house the gallium pellets (99.9999% purity - Alfa Aesar).

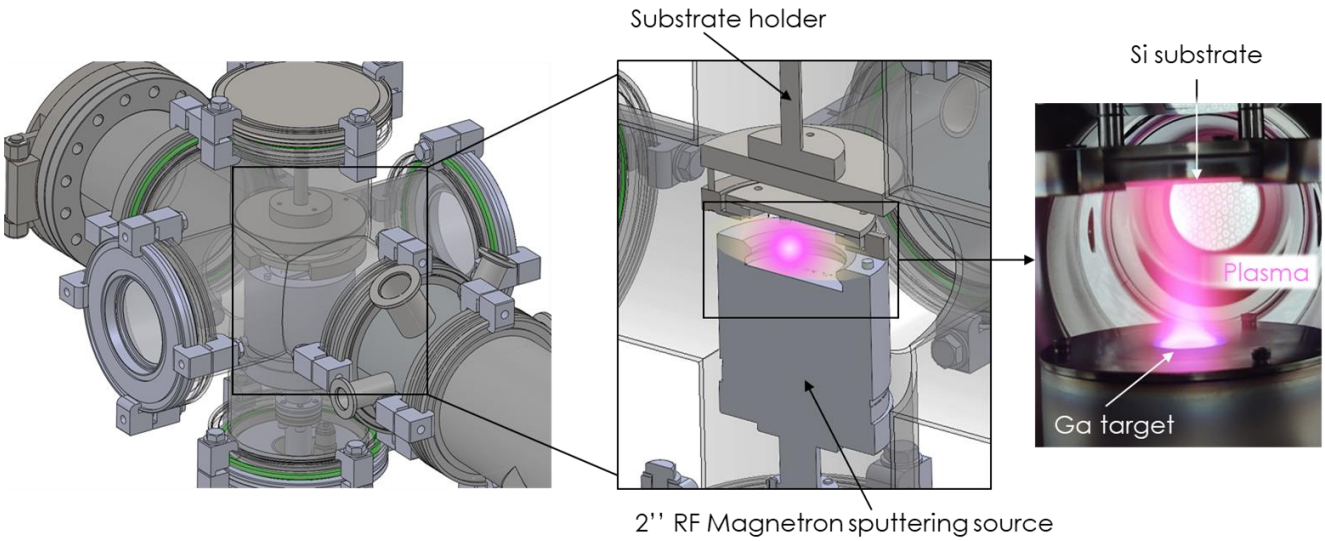

Figure 1. Overview of the sputtering reactor set-up used for GaN deposition.

The Ga pellets are melted to form a uniform layer of Ga that fills the designed target crucible made of stainless steel. The magnetron is powered by a 300 W - Radiofrequency (13.56 MHz) generator connected to an impedance matching box (TRUMPF PFG 300RF - Huttingter Elektronik). The gases (99.9999% purity Ar and N_2) are introduced in the chamber through a single hole inlet located at the bottom of the reactor. The system achieves a base vacuum pressure of about 10^{-7} mbar trough a dry pump (nXDS-10iR scroll Pump) and a turbo-molecular pump (Alcatel ATP-900). A butterfly valve is used to maintain the desired working pressure.

In this study, we focus on the effect of the working pressure, which we vary from 20 to 95 mTorr. The following conditions were kept fixed during deposition: (i) total gas flow of 7 sccm; (ii) Ar/N_2 flow ratio of 5:2; (iii) RF power of 100 W; (iv) n-type Si (100) wafers as substrates; (v) no substrate heating (depositions were carried out without intentional heating). We should mention that, under the conditions investigated here, the substrate heating that would have been induced by the plasma is fairly limited as thermocouple attached to the substrate holder indicated a temperature lower than 50°C when growing samples under a RF power of 100W on the target.

B. Characterization tools

To study the discharge, especially its efficiency in promoting Ga sputtering and more generally to get access to the species present in the plasma, optical emission spectroscopy (OES) was performed using an AVANTES Avaspec-ULS4096 CL-EVO spectrometer that has a slit width of 10 μm, a resolution (FWHM) of 0.7 nm and a spectral coverage in the UV-VIS region (from 200-750 nm).

When it comes to the analysis of the films grown, various *ex-situ* methods were used. The morphology and the thickness were analyzed using a Zeiss Merlin compact scanning electron microscope. The structure of the films was analyzed using a Panalytical Empyrean X-Ray Diffractometer (CuK_α radiation (λ=1.5406 Å). The polycrystalline nature of the films was revealed from grazing incidence (at 0.5°) X-ray diffraction (GIXRD) measurements carried out in the 2θ scan geometry. Along with GIXRD measurements, the structure of the thin films was analyzed using a Thermo Fisher Themis High-resolution Transmission Electron Microscope (HRTEM), working at 300 kV. For HRTEM, the films were scratched, and a residue was placed onto a carbon-coated copper grid. The structure of our samples was further studied using a Confocal Raman microscope (LABRAM HR Evolution) equipped with a 325 nm laser excitation source. The elemental profile of the deposited layers was analyzed using Secondary Ion Mass Spectrometry (SIMS) - IMS7f CAMECA. The IMS7f has a high sensitivity and excellent detection limits (10^{14} at.cm^{-3}) and has access to a high mass resolution ($M/\Delta M$=10000).

III. Results & discussion

A. Plasma analysis

In the sputtering process, Ar is primarily used for its heavy weight that will maximize the ejection of Ga-atoms, while N_2 is used as a source of N atom precursors in the gas phase. However, ensuring a high production of N-atoms is known to be challenging as the dissociation of N_2 is hard to achieve because of the strong triple bonding (941 kJ/mol) connecting the two atoms of the N_2 molecule[23]. The role of Ar in the discharge is therefore not only to perform the sputtering process; it may also participate in the enhancement of N-atom production through a resonant energy transfer channel with the Ar metastable species (Penning excitation)[24,25]. As a simple and non-intrusive way to identify the conditions that promote Ga sputtering while having strong emission of N_2, we used OES as a qualitative indicator. **Figure 2** shows the optical emission spectra of a pure Ar plasma (**A**), a pure N_2 plasma (**B**) and the Ar / N_2 plasma used for the deposition of GaN films (**C**).

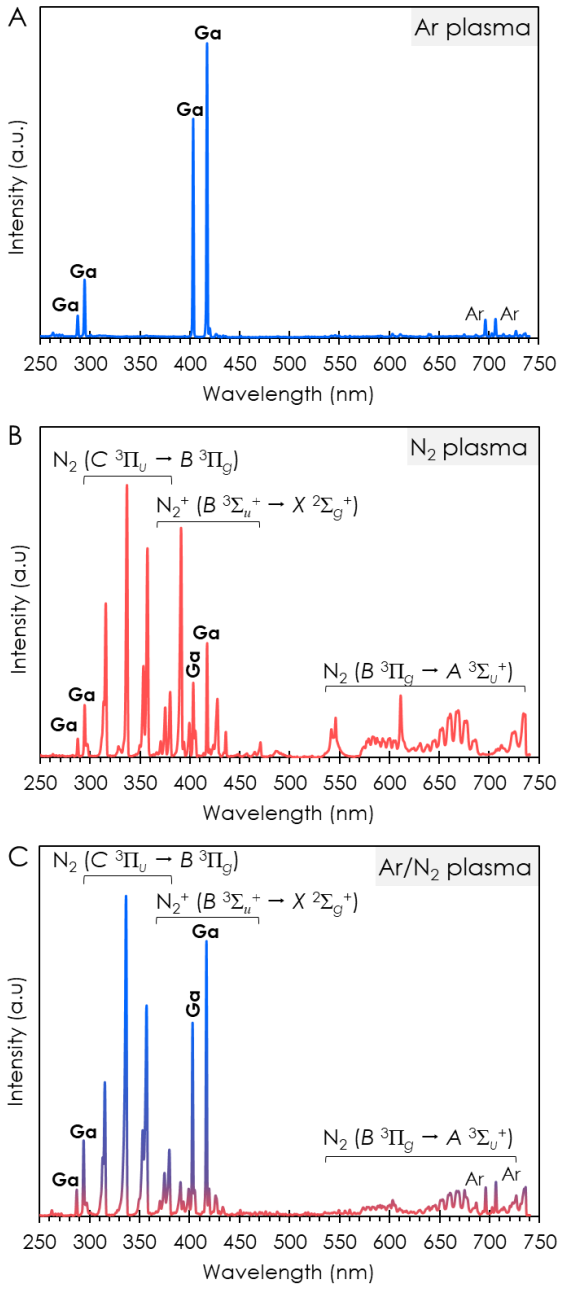

Figure 2. Optical emission spectra of: **A**: Ar plasma, depicting the atomic Ga lines; **B**: N_2 plasma, depicting the molecular and atomic nitrogen lines and atomic Ga lines and **C**: plasma with Ar/N_2 flow ratio of 5:2, showing strong atomic Ga lines along with the molecular nitrogen emission lines. *Sputtering conditions: 50 mTorr at 100 W.*

The main peaks on these spectra correspond to transition lines of molecular nitrogen, gallium and argon. The molecular features observed in **Figure 2.C** correspond to several transition lines from the N_2 second positive band system (SPS): $(C^3\Pi_u(v') \rightarrow B^3\Pi_g(v''))$, N_2^+ first negative system (FNS): $(B^2\Sigma_u^+(v') \rightarrow X^2\Sigma_g^+(v''))$ and N_2 first positive system (FPS): $(B^3\Pi_g(v') \rightarrow A^3\Sigma_u^+(v''))$, where v' and v'' are the vibrational quantum numbers of the upper and lower states[26]. The intense emission lines from SPS in the 300 to 370 nm region account for excitation and quenching processes from the ground state and the excitation from the first metastable state $N_2(A^3\Sigma_u^+)$ trough collision with Ar_m^* metastable species that implies the overpopulation of $N_2(C^3\Pi_u)$. In contrast, the peaks of both FNS are weaker, since the threshold energies for excitation from the FNS is much larger (~20 eV versus ~ 12 eV)[27]. The resonant transitions of Ga[28] are also evident in **Figure 2**. The sputtered Ga atoms in the Ar-N_2 plasma are excited into the metastable ($5s^2S_{1/2}$) level due to the collisions with the excited species and then decay radiatively with emissions at 403.3 and 417 nm[29] as observed in (**Figure 2.C**). The three spectra allow one to appreciate the interest in using Ar/N_2 mixture to enhance Ga sputtering instead of using solely N_2. Indeed, we observe that although pure N_2 plasma does induce Ga-atom ejection (**Figure 2.B**), the addition of Ar further promotes it along with a strong emission of N_2 (**Figure 2.C**). Even though OES provides only qualitative information, it has been verified by compositional analysis of the thin films using EDX, that the global ratio of the major Ga and N_2 lines gives a good approximation of the Ga/N ratio of the films. For example, the conditions at which the emission spectrum shown in **Figure 2.C** was acquired, gave quasi-stoichiometric thin films.

B. Thin film properties

Upon changing the various process parameters such as the pressure, RF power and gas flow, we found out that the working pressure had the strongest influence on the quality of the GaN thin films. In this study, we have only changed the working pressure and kept all the above-mentioned process parameters constant. It is well known that changing the working pressure results in the modification of the mean free path of the reactive species[30]. The longer the mean free path, the stronger the ion bombardment on the surface and hence the higher the adatoms mobility. Therefore, an efficient way to perform the analysis is to observe the evolution of the surface morphology as a function of the working pressure.

Figure 3.A-D shows SEM micrographs of thin films deposited at four different working pressures along with the respective cross-sectional images (**Figure 3.A'-D'**). Overall, from the top-view images, we observe that the films are nanostructured with feature sizes evolving as a function of the pressure. At 20 mTorr, we observe a surface with an irregular grain distribution. For pressure above 50 mTorr, the grain size is found to be in the range of 5-10 nm as observed in TEM images shown in **Figure 3.B"- C"**. In the cross-sectional images (**Figure 3.A'-B')**, a transition from a densely packed layer at 20 mTorr to a more columnar layer at 50mTorr is revealed. The columnar structure is also observed for the depositions at 75 and 95 mTorr as shown in **Figure 3.C'-D'**. In addition, all the deposited thin films exhibit a sharp and well-defined interface with the c-Si (100) substrate.

The effect of the working pressure on the morphology and structure of the thin films has been well established by Thornton's zone model[31]. At the lowest pressure of 20 mTorr (**Figure 3.A'**), the reactive species having higher energy in a less collisional regime, the mobility of adatoms on the substrate's surface is high enough to offset any self-shadowing effects, and produce a dense structure with little separation into individual columns[32].

When the process pressure is further increased to 50 and 75 mTorr, the kinetic energy of the reactive species decreases, producing a columnar structure (**Figure 3.B'-C'**). The lower migration of the atoms on the substrate's surface leads to the formation of columnar structures rather than a dense layer. At the highest working pressure of 95 mTorr (**Figure 3.D**), there is a drastic decrease in the grain size. The kinetic energy of the reactive species is the lowest, hence the adatoms mobility on the surface as well.

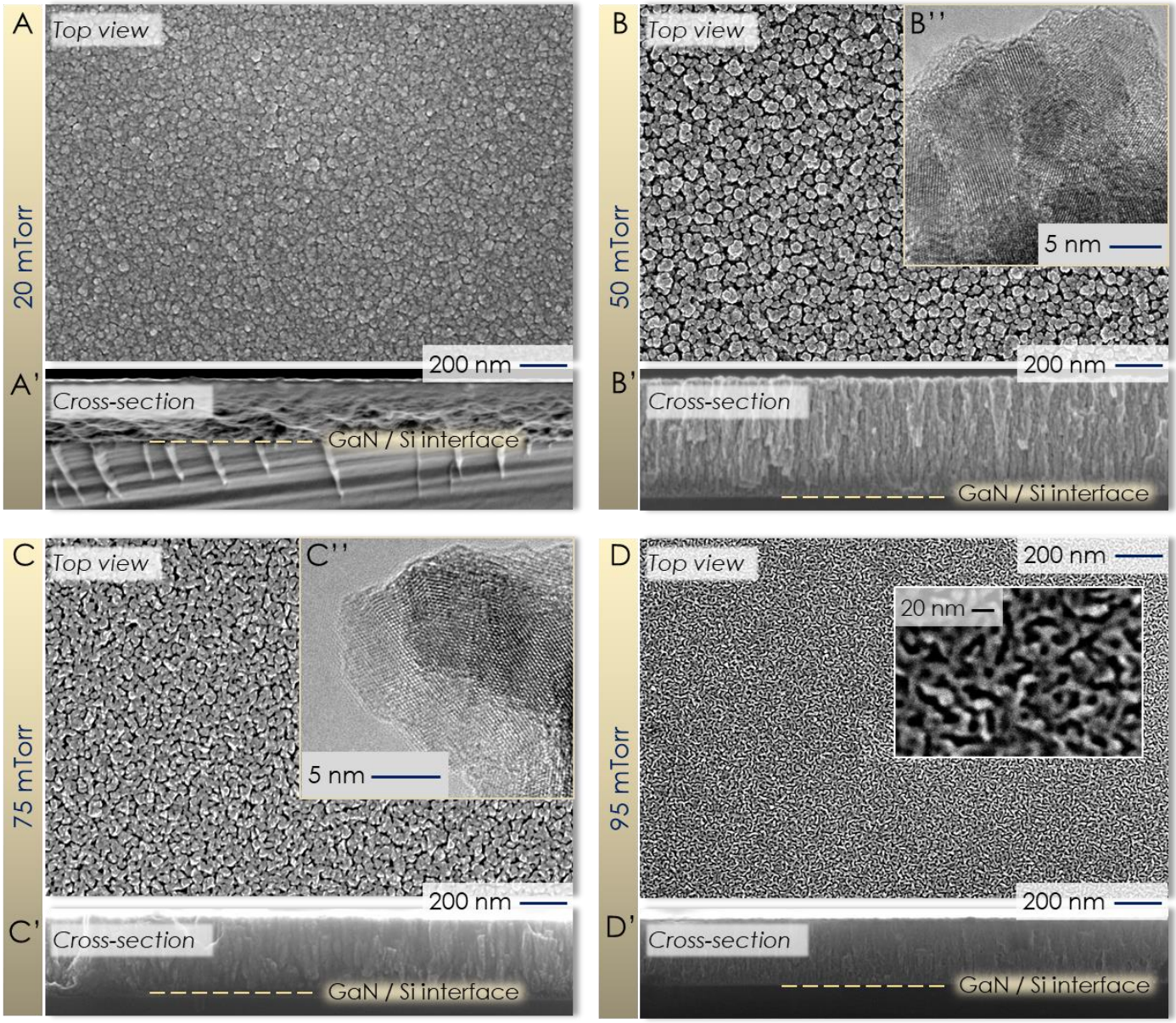

Figure 3. Top-view Surface, cross-sectional SEM and TEM (only for 50 and 75 mTorr) images of the GaN thin films deposited on c-Si(100) at various working pressures: **A,A'**: 20 mTorr; **B,B',B"**: 50 mTorr; 100W; **C,C',C"**: 75 mTorr and **D,D'**: 95 mTorr. The inset in **D** is a magnified part of the top view surface. *Sputtering conditions: Ar/N_2 flow ratio of 5:2 and power of 100 W*. **The scale is identical for top and cross-section views.**

To gain more insights on the deposition process, the growth rate as a function of the pressure has been estimated (**Figure 4**). Overall, the growth rate is of the order of a few Å/s with the highest growth rate achieved at 50 mTorr with a value of 2.87 Å/s. Such values are much higher than those reported for a GaN target and a pure Ar plasma (~ 0.4 Å/s)[33], whereas it is similar to a conventional deposition processes such as MBE that has an average growth rate of ~ 1-2 Å/s[34]. The variation of the growth rate can mainly be due to the flux of the reactive species that reach the surface. As the pressure is increased from 20 to 50 mTorr, the density of the reactive species in the discharge increases and hence their flux will increase, leading to a higher growth rate[35]. It almost doubles from ~1.52 Å/s to ~2.87 Å/s in the investigated pressure range. As the pressure is increased above 50 mTorr, one could expect to see an increase in the growth rate[35], but the opposite happens as the growth rate decreases from ~2.87 Å/s at 50 mTorr back to ~1.68 Å/s at 95 mTorr. In this case, it is important to consider that there are other factors that can be influenced by the working pressure.

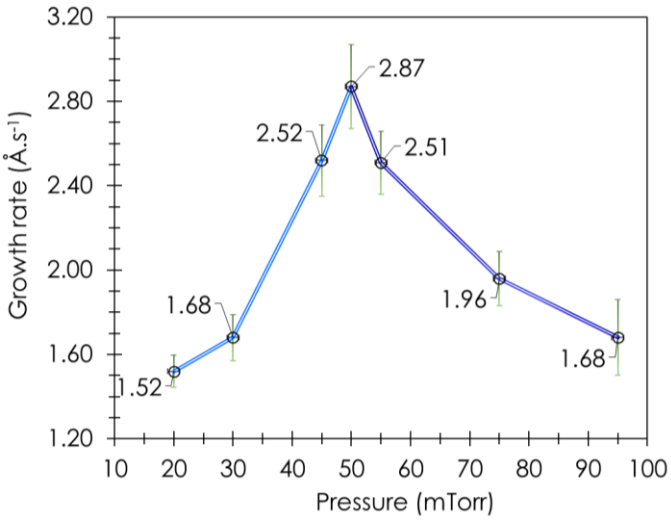

Figure 4. Growth rate of GaN thin films deposited on c-Si (100) as a function of working pressure. *Sputtering conditions: Ar/N_2 flow ratio of 5:2 and power of 100 W.*

For example, higher pressure conditions may result in an enhanced production of active nitrogen species in the plasma along with affecting the directionality of the metal flux from the target[36], leading to a decrease in the growth rate.

To determine the crystalline structure of the deposited material, Raman scattering spectroscopy has been employed to observe and identify the phonon modes of the GaN films. **Figure 5.A-D** shows the Raman spectra of the GaN samples deposited at four different working pressures. For a Raman system with a backscattering geometry such as the one used here, only the E_2 (high) and the A_1 (LO) modes are allowed, the others being forbidden[37]. **Table 1** presents the Raman spectra for the deposited thin films along with the reference data for the wurtzite and cubic zincblende structures of GaN.

Mode	Wurtzite GaN[37]	Cubic ZB GaN[37]	Experiment
E_2 (high)	569	552	564
A_1 (LO)	735	739	711

Table 1. Phonon modes in a wurtzite GaN, cubic zinc blende GaN and this experiment.

The Raman peak of the E_2 (high) phonon mode is prominently visible only for the samples grown at pressures greater than 20 mTorr. For the sample grown at 20 mTorr, this peak is not observed, while a broad peak centered around 680 cm^{-1} is observed, confirming the amorphous nature of the GaN film (**Figure 5.A**). For the other samples deposited at 50, 75 and 95 mTorr, the E_2(high) and A_1(LO) modes are clearly visible (**Figure 5.B-D)**. The peaks of the A_1(LO) mode at ~ 711 cm^{-1} are weak and deviate drastically with respect to the reference values of GaN at 735 cm^{-1}. Although the A_1(LO) mode is allowed, literature suggests that a quantitative analysis with this peak is hardly possible unless an epitaxial GaN layer is deposited[38]. The blue shift of both the E_2(high) and the A_1(LO) mode from a typical crystalline GaN layer may be attributed to numerous factors such as the strain, inhomogeneity in the chemical composition and structural defects[39].

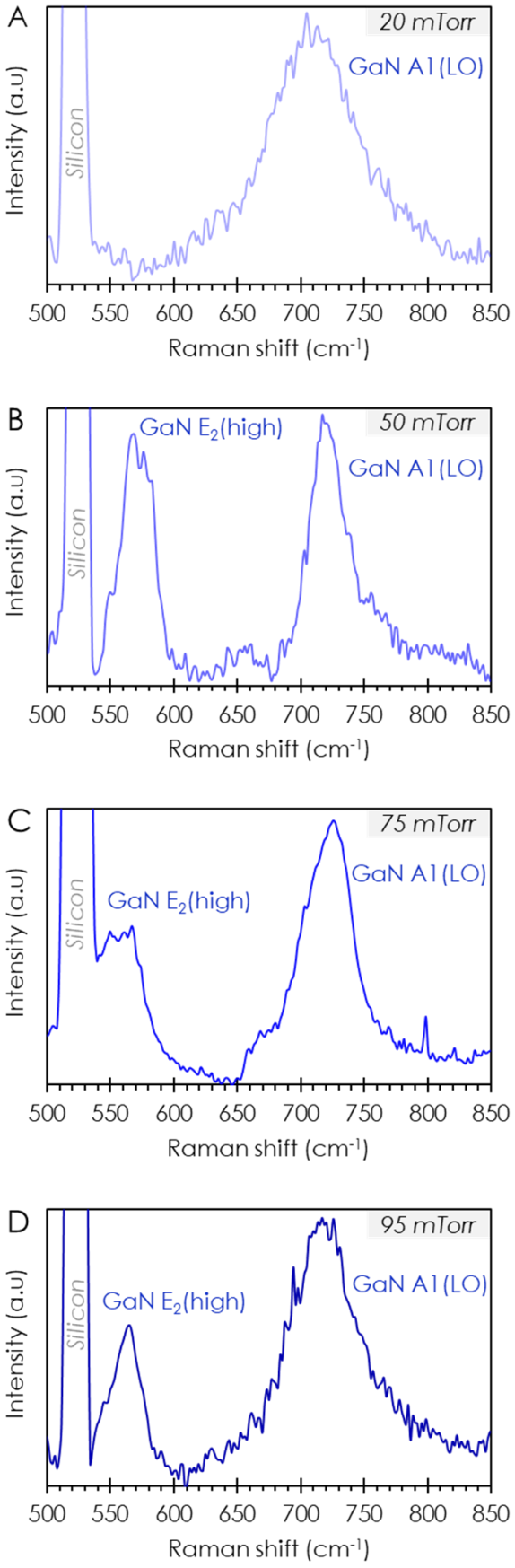

Figure 5. Raman spectra of the deposited GaN thin films on n-Si (100) at **A**: 20 mTorr; **B**: 50 mTorr; **C**: 75 mTorr and **D**: 95 mTorr. *Sputtering conditions: Ar/N_2 flow ratio of 5:2 and power of 100 W.*

Although the preceding Raman results are consistent with identifying the deposited layer as polycrystalline GaN, a more definitive technique is required to identify and analyze the crystallographic structure of the deposited thin films. Therefore, GIXRD was employed as shown in **Figure 6**.**A-D** in which the peak positions are those extracted from the JCPDS database[40]. The GIXRD patterns for the various working pressures (20 to 95 mTorr) are distinctive from 25-40°. A commonality on all these 4 spectrums are the weak broad peaks at 57°, 63° and 69° corresponding to the {11-20}, {10-13} and {11-22} crystal planes of hexagonal GaN.

The GIXRD pattern of the film deposited at 20 mTorr shows a broad spectrum from 30° to 40° and does not show any strong crystalline GaN peak (**Figure 6**.**A**). This suggests that the film deposited is amorphous and is in good agreement with the Raman results. For the sample deposited at 50 mTorr (**Figure 6**.**B**), a strong 0002 peak is observed at ~34°. When the working pressure is increased to 75 mTorr (**Figure 6**.**C**), two shoulder peaks alongside the 0002 peak at ~34° start to become more intense. These peaks are those of the {10-10} and {10-11} crystal planes of GaN, and the presence of all these peaks confirms that the GaN films have a dominant wurtzite hexagonal structure. However, as the relative intensity of these peaks does not match the powder spectrum of wurtzite, it is clear that some preferential orientation is present (although GIXRD does not directly allow one to identify it). For the polycrystalline samples (*i.e.* above 50 mTorr), we used the Sherrer's formula on the 0002 peak to estimate the grain size[41]. We have found that samples grown at 50, 75 and 95mTorr have grain size of ~ 9, 8 and 5 nm, respectively, which is in good agreement with the values observed in TEM images.

When the working pressure is increased from 50 to 75 and to 95 mTorr (**Figure 6.D**), the intensity of the 10-10 and 10-11 shoulder peaks becomes even stronger relative to the 0002 peak. This indicates that the degree and/or direction of preferential orientation depends on the process pressure. This may be explained by the energy model proposed by Losbichler & Mitterer[42], who link an anisotropy in growth rate along certain crystalline directions to the mobility of the impinging adatoms.

In **Figure 6**, one may also note some shifts between the measured peaks and their theoretical positions: the monotonous left-hand shift of all the peaks in **Figure 6.B** could indicate that the crystal parameter is slightly larger than the theoretical one in that case, while the shift of only the 0002 peak in **Figure 6.D** would indicate the presence of strain in this case. Let us note, however, that those shifts are significantly smaller than the peak width, so that, in each case, the crystal parameter and strain state most probably vary from one grain to the next.

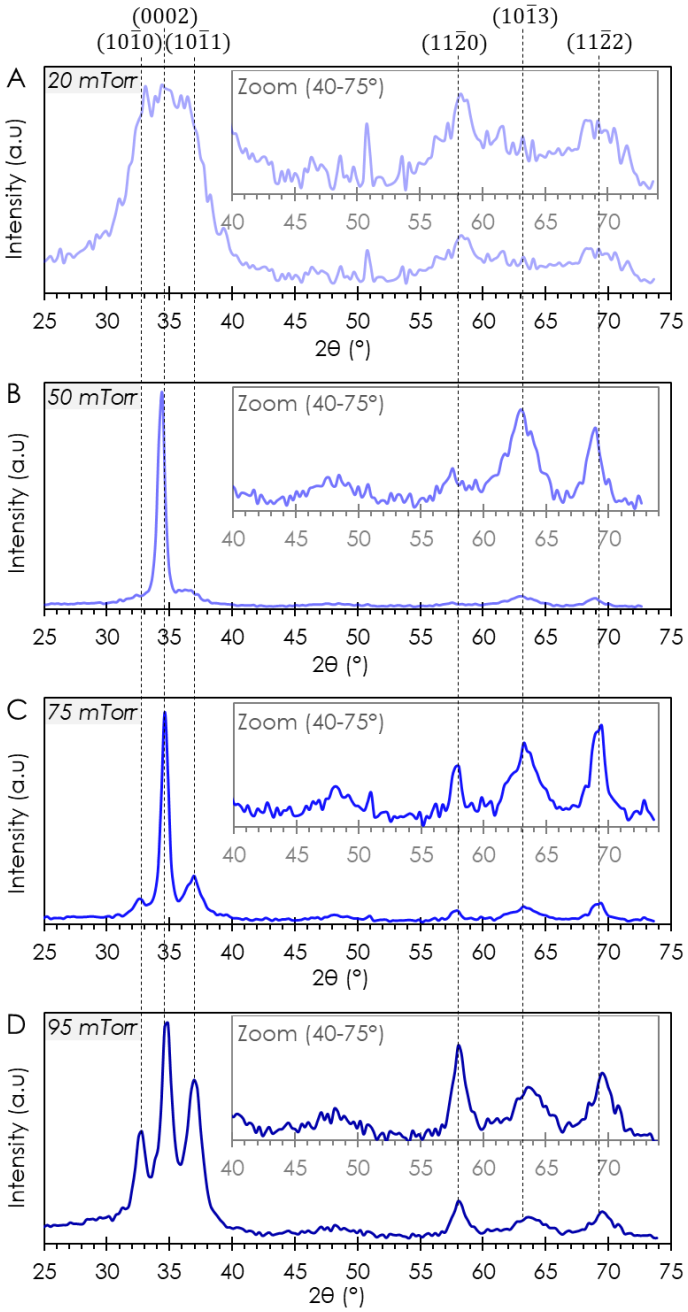

Figure 6. GIXRD patterns obtained at an incidence angle of 0.5° of the GaN thin films deposited on c-Si (100) at **A**: 20 mTorr; **B**: 50 mTorr; **C**: 75 mTorr and **D**: 95 mTorr. *Sputtering conditions: Ar/N_2 flow ratio of 5:2 and power of 100 W*. The insets correspond to a zoom of the 40-75° region.

Figure 7 shows the TEM images and structural analysis of a GaN flake obtained from a scratched portion of the thin film deposited at 50 mTorr. The high-resolution TEM (HR-TEM) images in **Figure 7.C-D** were obtained after tilting a flake in the microscope so that its growth axis is in the plane. In this geometric configuration, some grains were in a [11-20] zone axis (**Figure 7.D-E**), which allows one to directly see the stacking of the GaN (0002) compact planes oriented perpendicular to the growth direction.

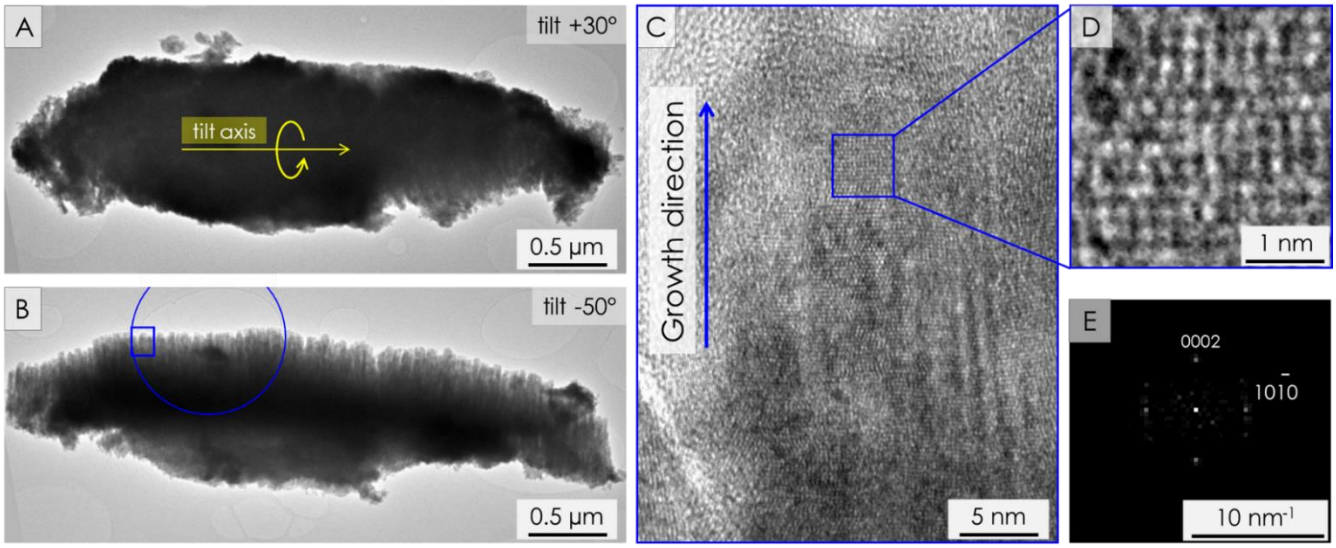

Figure 7. TEM of a GaN thin film grown at 50 mTorr.**A,B**: the sample, with its growth axis parallel to the electron beam at a tilt of +30° **(A)**, had that axis almost perpendicular to the beam (in the image plane) at a tilt of -50°**(B)** (*i.e.* at a total tilt of -80° with respect to **A**. The images in **Figure 7C-E** were recorded in the **B** orientation. The blue circle in **B** represents the selected area used for the diffraction pattern displayed in Figure 8. **C:** High-resolution image of the area blue-squared in **B**. **D:** Enlargement of the blue squared area in **C**, showing the stacking of the compact planes perpendicular to the growth direction. **E:** Fast Fourier transform (power spectrum) of **D** exhibiting a wurtzite stacking of those planes. *Sputtering conditions: Ar/N_2 flow ratio of 5:2 and power of 100 W.*

To confirm this texture effect on a larger scale, selected area diffraction patterns were recorded, as shown in **Figure 8**. The latter reveals a powder-pattern shape that confirms the polycrystalline nature of the GaN film, the reciprocal distance between the rings confirming in turn the wurtzite nature of the structure To try and qualify the texture detected by GIXRD, rotational average of the diffraction pattern[43] were performed around the growth direction on the one hand (red in **Figure 8**), and around an in-plane axis on the other hand (green in **Figure 8.B)**. The spectra in **Figure 8**.**B** evidence a strong presence of the 0002 peak in the former orientation (in red) and its absence in the latter (in green), indicating a strong [0001] texture.

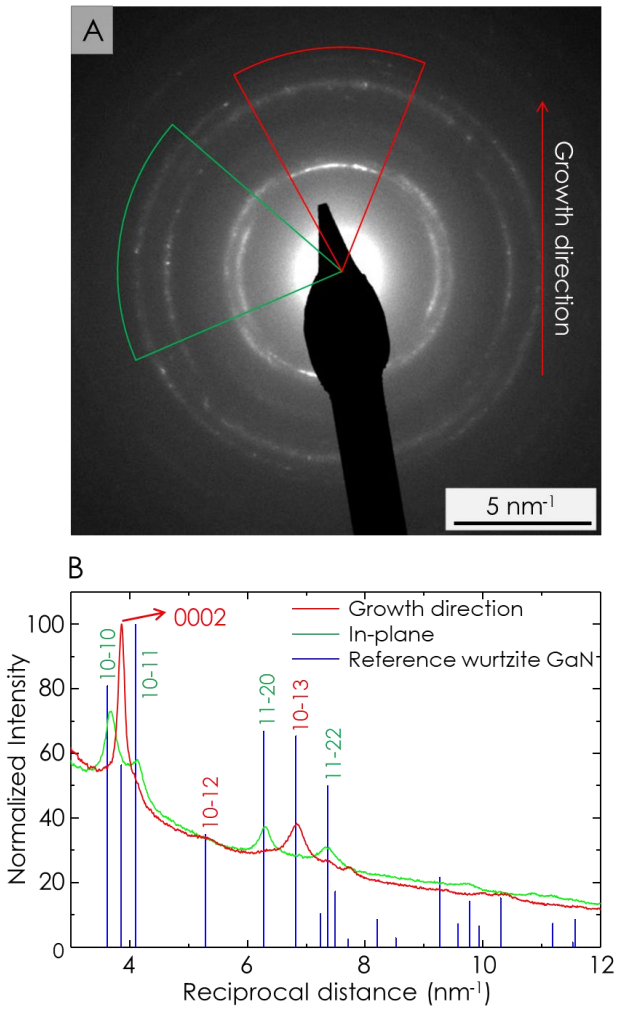

Figure 8. A: Electron diffraction pattern for the GaN sample deposited at 50 mTorr over the selected area shown by the blue circle in **Figure 7B**; the growth axis is almost in the plane, in the direction indicated. The red and green spectra in **B** represent the rotational averages from the red and green sectors in **A**, respectively, i.e. in the growth direction (red) and in the plane (green). *Sputtering conditions: Ar/N_2 flow ratio of 5:2 and power of 100 W.*

To evaluate the compositional profile along the growth direction of the film, secondary ion mass spectrometry (SIMS) was used. The cross-sectional SEM image of the GaN layer on c-Si (100) is shown in **Figure 9.A** and the corresponding SIMS profile is shown in **Figure 9.B**. The SIMS profile exhibits a nearly uniform presence of Ga and N throughout the film. At the interface with the c-Si substrate, an abrupt decrease in the Ga and N lines is observed. Consequently, a strong increase in the Si line is observed. Also, the sharp decrease in the Ga line at the interface depict that melt-back etching does not occur. The SIMS profile confirms the clean interface between GaN and c-Si which in agreement with the cross-sectional SEM micrograph (**Figure 9.A**). We should mention that a large amount of oxygen (up to 20% at.) is present in all the thin films as determined by EDX. This is very likely to come from residual water concentration in the chamber, which is significantly high as the reactor is, in its current form, not yet equipped with a load-lock system. We should mention that the O present in the films does not come from the target since Argon plasma cleaning (with shutter) is done prior to any deposition.

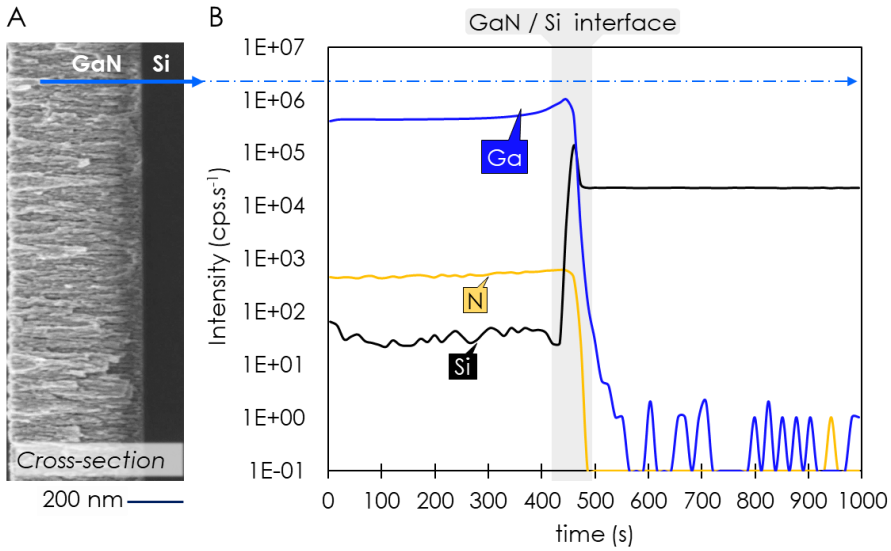

Figure 9. SEM cross section image of the GaN layer **(A)** and the SIMS composition profile (not quantitative) of the film deposited at 50 mTorr **(B)**. The arrow is a schematic representation of the cross-sectional profile of the probed region. *Sputtering conditions: Ar/N_2 flow ratio of 5:2 and power of 100 W. Remark: the SIMS measurement has not been calibrated so only the spatial distribution can be discussed here, the intensity being arbitrary.*

IV. Conclusion

Polycrystalline GaN thin films with a strong orientation towards the c-axis have been successfully grown on c-Si (100) substrates at room temperature using plasma-enhanced physical vapor deposition. The process conditions yielded a reasonable growth rate in the range of 1.4 ~ 2.9 Å /s, which is comparable to values obtained via a conventional processing method such as MBE. The surface morphology of the grown thin films showed microstructures with grain sizes in the range of a few tens of nm. X-ray diffraction peaks and Raman spectra identify the transition from an amorphous to a polycrystalline layer when the pressure is increased from 20 to 50 mTorr. The polycrystalline films have a hexagonal wurtzite GaN structure as confirmed TEM measurements. The best crystallinity and the highest growth rate are obtained at a working pressure of 50 mTorr. The elemental distribution of Ga and N is uniform through the film thickness and the GaN thin film has a sharp interface with the Si substrate. The films have a wurzite orientation and can be produced at reasonable growth rate, which makes them suitable for application as electron transport layer in solar cells, UV photodiodes, thin film transistors and flexible devices on thermos-sensitive substrates. Further work will target at studying the effect of the substrate temperature on the electronic properties and the used of advanced plasma diagnostics (TALIF) to better understand the effect of the process parameters on the film structure.

Acknowledgements

This research activity is supported by the ANR (Contract No. ANR-22-CE51-0011-01 and Contrat No. ANR-IEED-002-01). The authors thank Alexandre Blaizot and Francois Jomard for their valuable contributions in SEM and SIMS characterizations, respectively. TEM was carried out thanks to access to the Interdisciplinary Center for Electron Microscopy of Ecole Polytechnique (CIMEX).

Conflict of Interest

The authors declare no conflict of interest.

Data availability

The data that support the findings of this study are available from the corresponding author upon reasonable request.

References

1) S. Nakamura, T. M. Takashi Mukai and M. S. Masayuki Senoh, Jpn. J. Appl. Phys. **30**, L1998 (1991).
2) S. Nakamura, M. Senoh, S. Nagahama, N. Iwasa, T. Yamada, T. Matsushita, H. Kiyoku, Y. Sugimoto, T. Kozaki, H. Umemoto, M. Sano and K. Chocho, Jpn. J. Appl. Phys. **37**, L309 (1998).
3) S. C. Binari, W. Kruppa, H. B. Dietrich, G. Kelner, A. E. Wickenden and J. A. Freitas, Solid-State Electron. **41**, 1549 (1997).
4) S. Strite, J. Vac. Sci. Technol. B Microelectron. Nanometer Struct. **10**, 1237 (1992).
5) M. Ishida, T. Ueda, T. Tanaka and D. Ueda, IEEE Trans. Electron Devices **60**, 3053 (2013).
6) A. Krost and A. Dadgar, Phys. Status Solidi A **194**, 361 (2002).
7) E. Arslan, M. K. Ozturk, A. Teke, S. Ozcelik and E. Ozbay, J. Phys. Appl. Phys. **41**, 155317 (2008).
8) M. Sobanska, K. Klosek, Z. R. Zytkiewicz, J. Borysiuk, B. S. Witkowski, E. Lusakowska, A. Reszka and R. Jakiela, Cryst. Res. Technol. **47**, 307 (2012).
9) M. Tautz and D. Díaz Díaz, Chemistry Select **3**, 1480 (2018).
10) C. M. Furqan, J. Y. L. Ho and H. S. Kwok, Surf. Interfaces **26**, 101364 (2021).
11) E. Gastellóu, G. García, A. M. Herrera, C. Morales, R. García, G. A. Hirata, E. Rosendo, J. A. Luna, M. Robles, J. A. Rodríguez and Y. D. Ramírez, Appl. Sci. [DOI:10.3390/app11156990].
12) M. Monish, S. Mohan, D. S. Sutar and S. S. Major, Semicond. Sci. Technol. **35**, 045011 (2020).
13) M. Simanullang, Z. Wang, N. Kawakami, R. Ogata, T. Yoshida and M. Sugiyama, Thin Solid Films **675**, 1 (2019).
14) R. Fukamizu, N. Aso, Y. Shiratori and S. Miyajima, Jpn. J. Appl. Phys. **62**, SK1035 (2023).
15) M. Junaid, C.-L. Hsiao, J. Palisaitis, J. Jensen, P. O. Å. Persson, L. Hultman and J. Birch, Appl. Phys. Lett. **98**, 141915 (2011).
16) D. C. Park, Sz. Fujita and Sg. Fujita, Phys. Status Solidi A **176**, 579 (1999).
17) G. N. Chaudhari, V. R. Chinchamalatpure and S. A. Ghosh, Am. J. Anal. Chem. **02**, 984 (2011).
18) H.-D. Xiao, R. Liu, J.-Q. Liu, Z.-J. Lin and L.-M. Mei, Vacuum **83**, 1393 (2009).
19) K. S. A. Butcher, H. Timmers, Afifuddin, P. P.-T. Chen, T. D. M. Weijers, E. M. Goldys, T. L. Tansley, R. G. Elliman and J. A. Freitas, J. Appl. Phys. **92**, 3397 (2002).
20) H. Wei, J. Wu, P. Qiu, S. Liu, Y. He, M. Peng, D. Li, Q. Meng, F. Zaera and X. Zheng, J. Mater. Chem. A **7**, 25347 (2019).
21) P. Qiu, H. Wei, Y. An, Q. Wu, W. Du, Z. Jiang, L. Zhou, C. Gao, S. Liu, Y. He, Y. Song, M. Peng and X. Zheng, Ceram. Int. **46**, 5765 (2020).
22) S. Banerjee, A. A. I. Aarnink, D. J. Gravesteijn and A. Y. Kovalgin, J. Phys. Chem. C **123**, 23214 (2019).
23) I. Sugimoto, S. Nakano and H. Kuwano, J. Appl. Phys. **75**, 7710 (1994).
24) J. Muñoz, J. Margot and M. Chaker, J. Phys. Appl. Phys. **46**, 455205 (2013).
25) W. Park, J. Han, J. Kim and S. Y. Moon, Thin Solid Films **764**, 139629 (2023).
26) T. H. Chung, Y. W. Lee, H. M. Joh and M. A. Song, AIP Adv. **1**, 032136 (2011).
27) P. N. Stanton and R. M. St. John, J. Opt. Soc. Am. **59**, 252 (1969).
28) T. Shirai, J. Reader, A. E. Kramida and J. Sugar, J. Phys. Chem. Ref. Data **36**, 509 (2007).
29) C. Corr, R. Boswell and R. Carman, J. Phys. Appl. Phys. **44**, 045201 (2011).
30) D. G. Teer, Surf. Coat. Technol. **39**, 565 (1989).
31) J. A. Thornton, in *Modeling of Optical Thin Films* (SPIE, 1988) Vol. 821 pp. 95.
32) E. Alfonso, J. Olaya and G. Cubillos, in *Crystallization - Science and Technology*, ed. M. Andreeta (InTech, 2012).
33) H. F. Huq, R. Y. Garza and R. Garcia-Perez, J. Mod. Phys. **07**, 2028 (2016).
34) Z. Yang, L. K. Li and W. I. Wang, Appl. Phys. Lett. **67**, 1686 (1995).
35) P. K. Song, E. Yoshida, Y. Sato, K. H. Kim and Y. Shigesato, Jpn. J. Appl. Phys. **43**, L164 (2004).
36) A. Prabaswara, J. Birch, M. Junaid, E. A. Serban, L. Hultman and C.-L. Hsiao, Appl. Sci. **10**, 3050 (2020).
37) V. Lemos, C. A. Argüello and R. C. C. Leite, Solid State Commun. **11**, 1351 (1972).
38) A. G. Milekhin, R. J. Meijers, T. Richter, R. Calarco, S. Montanari, H. Lüth, B. A. P. Sierra and D. R. T. Zahn, J. Phys. Condens. Matter **18**, 5825 (2006).

39) M. S. Kumar and J. Kumar, Mater. Chem. Phys. **77**, 341 (2003).
40) R. Jenkins, T. G. Fawcett, D. K. Smith, J. W. Visser, M. C. Morris and L. K. Frevel, Powder Diffr. **1**, 51 (1986).
41) A. L. Patterson, Phys Rev **56**, 978 (1939).
42) P. Losbichler and C. Mitterer, Surf. Coat. Technol. **97**, 567 (1997).
43) D. R. G. Mitchell, Microsc. Res. Tech. **71**, 588 (2008).